PCCP

PAPER

View Article Online
View Journal | View Issue

Cite this: *Phys. Chem. Chem. Phys.*, 2016, **18**, 11297

A density functional theory study of arsenic immobilization by the Al(III)-modified zeolite clinoptilolite

Joel B. Awuah,[a] Nelson Y. Dzade,*[b] Richard Tia,[c] Evans Adei,[c] Bright Kwakye-Awuah,[a] C. Richard A. Catlow[de] and Nora H. de Leeuw[bde]

Received 11th January 2016,
Accepted 21st March 2016

DOI: 10.1039/c6cp00190d

www.rsc.org/pccp

We present density functional theory calculations of the adsorption of arsenic acid ($AsO(OH)_3$) and arsenous acid ($As(OH)_3$) on the Al(III)-modified natural zeolite clinoptilolite under anhydrous and hydrated conditions. From our calculated adsorption energies, we show that adsorption of both arsenic species is favorable (associative and exothermic) under anhydrous conditions. When the zeolite is hydrated, adsorption is less favourable, with the water molecules causing dissociation of the arsenic complexes, although exothermic adsorption is still observed for some sites. The strength of interaction of the arsenic complexes is shown to depend sensitively on the Si/Al ratio in the Al(III)-modified clinoptilolite, which decreases as the Si/Al ratio increases. The calculated large adsorption energies indicate the potential of Al(III)-modified clinoptilolite for arsenic immobilization.

1. Introduction

Arsenic is recognized as one of the most toxic contaminants in the environment, harmful for humans and other living organisms.[1] It is released into the environment mostly through natural processes, due to the presence and dissolution of arsenic-containing minerals, volcanic emissions and from geothermal sources, and also as a consequence of anthropogenic activities, including mining, combustion of fossil fuels and the use of arsenic-containing pesticides.[2] The effects of arsenic on human health are highly detrimental, with arsenic poisoning having been linked to neurological disorders, dermatological and gastro-intestinal problems,[3] and it is a known carcinogen.[4] To alleviate the health impact of arsenic, the United States Environmental Protection Agency (USEPA) has revised the maximum contaminant level (MCL) from 50 to 10 ppb in drinking water.[5]

The most prevalent valence states of arsenic in water are arsenate, As(v), and arsenite, As(III).[6] The latter is more toxic (20–65 times) and more mobile (being able to travel five to six times faster) than the former and is one of the main toxic species in natural waters.[1,7,8] An understanding of the geochemistry of arsenic in low temperature anoxic sedimentary environments is therefore crucial to the development of safe drinking water and food supplies.[9,10] Of the processes controlling arsenic mobility, adsorption onto mineral surfaces is thought to strongly influence its concentrations in aquatic environments.[11] Iron oxide minerals such as magnetite, goethite and hematite have been widely used as sorbents to remove contaminants in the form of arsenic oxyanions from wastewater and soils. Their removal has been attributed to ion exchange, specific adsorption onto surface hydroxyl groups, or co-precipitation.[9,12–14]

Natural zeolites, which are environmentally and economically viable hydrated aluminosilicates, with exceptional ion-exchange and sorption properties, have recently been explored as potential materials for the removal of arsenic from wastewater.[15–17] Their unique three-dimensional porous structural framework makes natural zeolites suitable for applications in industrial adsorptive and ion exchange processes. Because of the excess negative charge on the surface of the zeolite, which results from an isomorphic replacement of silicon by aluminum in the primary structural units, natural zeolites belong to the group of cation exchangers. A number of earlier studies have confirmed their excellent performance in the removal of metal cations from wastewaters.[18–21]

Among the natural zeolites, clinoptilolite (CL) is considered one of the most promising candidates for use in the decontamination and removal of arsenic and high-level heavy metal wastes owing to its unique physical and chemical properties, *i.e.* its cation

[a] *Department of Physics, Kwame Nkrumah University of Science and Technology, Kumasi, Ghana*
[b] *Department of Earth Sciences, Utrecht University, Princetonplein 9, Utrecht, 3584 CC, The Netherlands. E-mail: N.Y.Dzade@uu.nl, N.H.Deleeuw@uu.nl*
[c] *Department of Chemistry, Kwame Nkrumah University of Science and Technology, Kumasi, Ghana*
[d] *Department of Chemistry, University College London, 20 Gordon Street, WC1H 0AJ, UK*
[e] *School of Chemistry, Cardiff University, Main Building, Park Place, Cardiff CF10 3AT, UK*

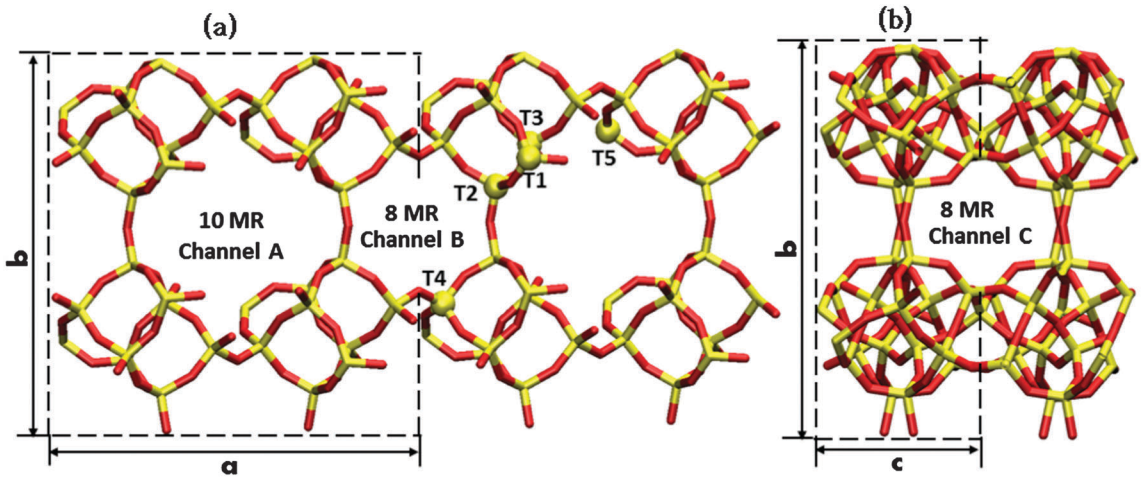

Fig. 1 The siliceous clinoptilolite framework showing the channels of the 10-and 8-membered rings (MR) in a repeat unit cell. The five distinct tetrahedral sites in the framework for Al atoms substitution are labelled T_i (i = 1–5) according to ref. 43. The primitive cell is highlighted by dashed lines (Si = yellow, O = red).

exchange capacity, large specific internal surface area and adsorptive affinity for organic and inorganic ions.[22] CL is the best known natural zeolite; it can be found in large deposits worldwide and has a relatively low extraction cost. Clinoptilolite crystallizes in the monoclinic cell structure with the space group $C2/m$. The framework is of HEU (Heulandite) type and exhibits a Si/Al ratio between 4.5 and 5.5.[1] The porous structure of clinoptilolite is characterized by a 2-dimensional network of three channels, as shown in Fig. 1. Channels A and B run along the c-axis and exhibit 8- and 10-membered rings, respectively, whereas channel C also contains 8-membered rings and runs parallel to the a-axis. These channels can host up to 20 water molecules per unit cell and a number of extra-framework/exchangeable cations such as Na^+, K^+, and Ca^{2+}.[23,24] The cation site preference in zeolite clinoptilolite has recently been investigated by Uzunova and Mikosch[25] using density functional calculations, who showed that configurations with Al → Si substitution at the T2 site, which interconnects the xz layers *via* its apical oxygen atom, are the most stable ones, in agreement with experimental data.[26] The configurations with Al → Si substitution at the T1 sites were demonstrated to favour the migration of cations from the eight-membered rings into the large channel A of the ten-membered ring (Fig. 1); the process is energetically the most favorable for the Na^+ cations.[25] The favourable energetics for cation migration into the ten-membered A ring can be attributed to its large pore size (opening 7.05 × 4.25 Å, *ca.*) compared to the smaller eight-membered B ring (opening 4.6 × 3.96 Å, *ca.*).[27,28] In light of its large pore site and favourable cation migration thermodynamics, the ten-membered A ring has high occupancy towards alkaline metals than the eight-membered ring.[25]

In common with all zeolites, the negatively charged surface causes clinoptilolite to be unsuitable for the binding of anionic species.[29] However, chemical modification of the surface would allow clinoptilolite to become an effective sorbent for oxyanions.[30] For example, it has been reported recently that natural clinoptilolite could be a suitable carrier for salicylate anions.[31] Also, it has been shown that iron(III)-modified natural clinoptilolite effectively removes arsenite and arsenate ions from aqueous solutions.[32] Due to its non-toxic, ecological and natural abundance, and unique physico-chemical properties, natural clinoptilolite has also been considered as a carrier for fertilizers employed in plant growth, owing to its propensity to gradually release nutrients.[33]

In view of the potential of clinoptilolite for As removal from water, the aim of the present study was to employ density functional theory techniques to investigate the adsorption mechanisms of arsenic acid $AsO(OH)_3$ and arsenous acid $As(OH)_3$ in the Al(III)-modified clinoptilolite zeolite. We present and discuss in detail information on the local structure of the adsorption complexes under vacuum and hydrated conditions and the adsorption mechanism within the Al(III)-containing CL zeolite framework. Different Si/Al ratios have been explored and shown to have significant effects on the adsorption properties of $AsO(OH)_3$ and $As(OH)_3$.

2. Computational methods

Density functional theory (DFT) calculations within the generalized gradient approximation (GGA)[34] were carried out using the plane-wave pseudopotential PWSCF code in the Quantum-ESPRESSO package.[35] We used ultrasoft pseudopotentials[36] with the PBE functional[37] to represent the potential of the nuclei and core electrons of the atoms, and a plane-wave basis with an energy cut-off of 30 Ryd to represent the Kohn–Sham wavefunctions. This energy cut-off was tested to be sufficient to converge the total energy of the clinoptilolite system to within 0.0001 Ry. Integration over the Brillouin zone was carried out using the Monkhorst–Pack scheme[38] with a 1 × 1 × 1 mesh of k-points, and occupation numbers were treated according to the Methfessel–Paxton[39] scheme with a broadening of 0.003 Ry. The very large unit cell of clinoptilolite (a = 17.5 Å, b = 17.6 Å, c = 7.4 Å) justifies the use of a 1 × 1 × 1 k-point mesh to accurately describe the structural parameters. Structural relaxation was carried out in

each case to minimize the energy using the conjugate gradient method using the Broyden–Fletcher–Goldfarb–Shanno (BFGS) algorithm,[40] until the magnitude of the residual Hellmann–Feynman force on each relaxed atom reached 0.01 eV $Å^{-1}$.

The purely siliceous clinoptilolite was modelled in the monoclinic structure (space group $C2/m$),[41] consisting of 108 atoms with the general formula $Si_{36}O_{72}$. Full geometry optimization was performed on the initial structure to obtain the relaxed unit cell parameters and the interatomic bond distances and angles. Having obtained the relaxed structure of the purely siliceous clinoptilolite zeolite, some of the Si atoms were substituted by Al atoms, beginning from the Si atoms at various tetrahedral sites in the pores, leading to a Si/Al ratio in the range of 1.7–8.0, following both Löwenstein's rule,[42] where no Al–O–Al linkage is permitted, and Dempsey's rule for maximum separation of negative framework charges.[43] Further geometry optimizations were performed following the substitution of Si by Al in order to obtain optimized structural parameters of bond distances and angles in the substituted clinoptilolite systems. Sodium cations were inserted to compensate for the charge of each inserted Al, by placing it in the same plane as the Al and two randomly selected oxygen to which the Al is bonded. All graphical representations of structures in this paper have been prepared using XCRYSDEN[44] and visual molecular dynamics (VMD)[45] software.

3. Results and discussion

3.1 Pure clinoptilolite structure

The monoclinic primitive cell of pure clinoptilolite (dashed lines) showing the 10-and 8-membered ring (MR) channels in a repeat cell is displayed in Fig. 1. The five distinct tetrahedral sites in the framework for a partially random distribution of Al atoms, labelled T_i (i = 1–5) following Margeta and Logar,[15] are also identified. Our calculated lattice parameters, the interatomic bond distances and angles of the purely siliceous CL are summarized in Table 1, and they show excellent agreement with experimental data[46] and previously calculated DFT values.[47] The Si–O bond distance is only slightly overestimated with respect to typical experimental values, ~1.605 Å.[26] However, such an overestimation is a well-documented deficiency of the DFT methodology in the description of Si–O bonds.[47–49]

3.2 Anhydrous and hydrated Al-modified clinoptilolite

The framework density of purely siliceous clinoptilolite ($Si_{36}O_{72}$) is low at 17.7 T/1000 $Å^3$ with five different tetrahedral sites as shown in Fig. 1.[52] Substituting some of the tetrahedral Si atoms by Al creates a negatively charged framework and thus requires charge-compensation by extra-framework cations within the cages and channels; typically alkali metals and alkaline earth elements (*e.g.*, Na^+, K^+, Ca^{2+}, Ba^{2+}, Sr^{2+}, Cs^+, and Mg^{2+}) are included.[50] In this study, Na^+ is used to compensate for the negative charge resulting from the Si → Al substitution. Different Al/Si ratios were considered (1.7–8.0) and, in each composition, we have modelled the anhydrous and hydrated systems. For the hydrated systems, five water molecules were added in extra-framework positions yielding the general formula $(A^+z)y/z(Al^{3+})y(Si)xO_2(x+y)\cdot nH_2O$, where A represents the extra-framework cations, z is the charge on the extra-framework cations, n is the number of molecules of molecular water, and x and y are the stoichiometric coefficients for Al^{3+} and Si^{4+} in tetrahedral sites, respectively. In Table 2, we report the fully optimized structural parameters for different Si/Al ratios of CL, for both the anhydrous and hydrated compositions.

In the anhydrous Al-modified CL (Fig. 2a), we found that the distribution of the Na^+ cations in the framework is clustered around the negatively charged framework oxygens at an average distance of 2.34 Å. The average Si–O bond distance was calculated at 1.643 Å (Table 2), which, when compared to the average purely siliceous system (1.605 Å), represents an elongation. The Al–O bond calculated at 1.777 Å is found to be longer than the Si–O bond distance, as expected. The TOT angles in proximity to the cation sites undergo strong deformation (125.3°–154.5°) as shown in Table 2, which is consistent with an earlier DFT result of Uzunova and co-workers.[25]

In the hydrated Al-modified CL, the water molecules were inserted to coordinate the extra framework cations by placing them at an average Na^+–O_{water} distance of 2.52 Å so that they can easily interact with the Na^+ cations. The starting positions of the water molecules were at realistic distances from the zeolite framework and comparable with the cation–water distances obtained from experimental data (2.4–2.9 Å).[53,54] From the optimized average coordinates, we found that each water molecule is coordinated to at least two Na cations, at an average distance of 2.37 Å within the 10-membered rings at positions denoted M1 in channel A, as shown in Fig. 2b. Our DFT calculated average Na^+–O_{water} distances and the water orientations compare reasonably well with those obtained from classical molecular dynamics (MD) simulations (2.29–2.41)[55,56] and experimental data for clinoptilolite[53] and other zeolite frameworks.[54] Similar cation–O_{water} distances were obtained when classical energy minimization techniques were employed to model the effect of hydration on the adsorption behavior of extra-framework cations in zeolite A.[57] The good agreement of our calculated Na^+–O_{water} distances with those obtained from MD simulations and experimental findings gives us confidence that the interactions between water, extra-framework cations and the zeolite framework are modelled accurately by the DFT approach.

For the clinoptilolite with a Si/Al ratio of 5, three of the Na^+ cations occupy the M1 site (M1a, M1b, and M1c). As shown in Fig. 2(b1), M1c is located close to the T2–O–T2 linkage, while both the M1a and M1b are located close to T5, with a bond

Table 1 Pure siliceous clinoptilolite unit cell parameters (Å), average bond distances (Å), and angles (°), in comparison with experimental and previous DFT results

Parameter	Expt.[46,50,51]	This work	PBE[47]	PBEO[47]
a	17.50	17.52	17.53	17.48
b	17.60	17.64	17.77	17.69
c	7.40	7.40	7.42	7.39
Si–O	1.61	1.62	1.64	1.62
⟨O–Si–O⟩		109.3	109.5	109.4
⟨Si–O–Si⟩		142.7	142.6	144.6

Table 2 Structural parameters including bond lengths (Å) and bond angles between tetrahedral sites (°) of anhydrous and hydrated clinoptilolite at different Si/Al ratios. R_{MO} denote Na^+-framework oxygen distances

	Si/Al = 1.7		Si/Al = 5		Si/Al = 6		Si/Al = 8		Theory[25]
Parameter	Anhydrous	Hydrated	Anhydrous	Hydrated	Anhydrous	Hydrated	Anhydrous	Hydrated	Anhydrous
Si–O	1.643	1.648	1.612	1.614	1.591	1.602	1.600	1.721	1.656
Al–O	1.777	1.761	1.748	1.745	1.744	1.722	1.723	1.609	1.763
R_{MO}	2.320	2.234	2.439	2.367	2.339	2.365	2.340	2.391	2.325
T2-O-T2	143.8	150.0	139.6	147.7	151.4	154.5	152.0	152.7	147.2
T2-O-T3	138.4	137.5	138.9	143.2	146.2	143.5	150.7	142.6	140.5
T2-O-T1	130.0	131.9	126.5	125.3	128.7	136.9	129.1	131.5	135.2

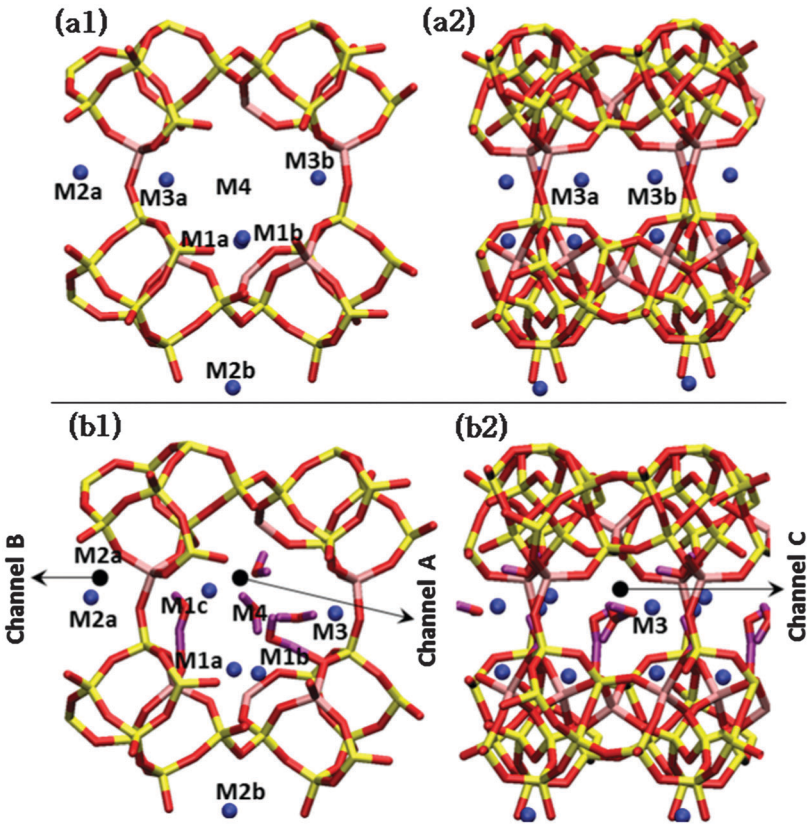

Fig. 2 The structure of anhydrous (a1 & a2) and hydrated (b1 & b2) Al-modified clinoptilolite viewed along the [001] direction (1), and the [100] direction (2), showing the preferred sites of the charge-compensating Na^+ cations. (Si = yellow, O = red, Al = pink, Na = blue, H = violet).

length of 2.96 Å between them. In the mix of other cations (such as Na^+, Ca^{2+}, K^+, Mg^{2+} and Ba^{2+}), this site can be occupied by Ca^{2+} but preferably by Na^+.[26] Site M2 is located in channel B, coordinated by oxygen atoms from the 8 MR. This site is occupied by two Na^+ cations, M2a and M2b. M2a is located close to the T2–O–T2 linkage, while M2b is shifted towards the centre of the ring. With other cations included in the framework, M2 is occupied by Na^+ and preferably Ca^{2+}.[26] Site M3 located in channel C is coordinated by the framework oxygen from the 8 MR in the (100) plane and one H_2O molecule (2.26 Å).

The M3 site is occupied by only one Na^+ cation. This site can also be occupied by K^+, and probably Ba^{2+}, in the presence of other cations.[26] Because this site is very close to M1, a simultaneous occupancy of both sites is not possible.[25] M4 is the fourth site which is located in the centre of channel A but is different from M1. The occupancy of this site is low, usually by Mg^{2+},[26] but from our calculations we did not find a Na^+ cation occupying this site. Experimental studies on a hydrated Al-modified clinoptilolite have reported these sites as the lowest energy occupancy sites.[26]

Fig. 3 shows the isosurface of the charge density of the hydrated and anhydrous Al-modified CL zeolite with a Si/Al ratio of 5. Compared to the anhydrous case (Fig. 3(a)), the charge density distribution within the pores is reduced in the hydrated frameworks (see Fig. 3(b)), and the presence of water in the CL zeolite framework thus appears to serve as a charge delocalizer. Charge density affects the location of molecules in the lattice, where more polar molecules will occupy the sites within the lattice with high charge density.

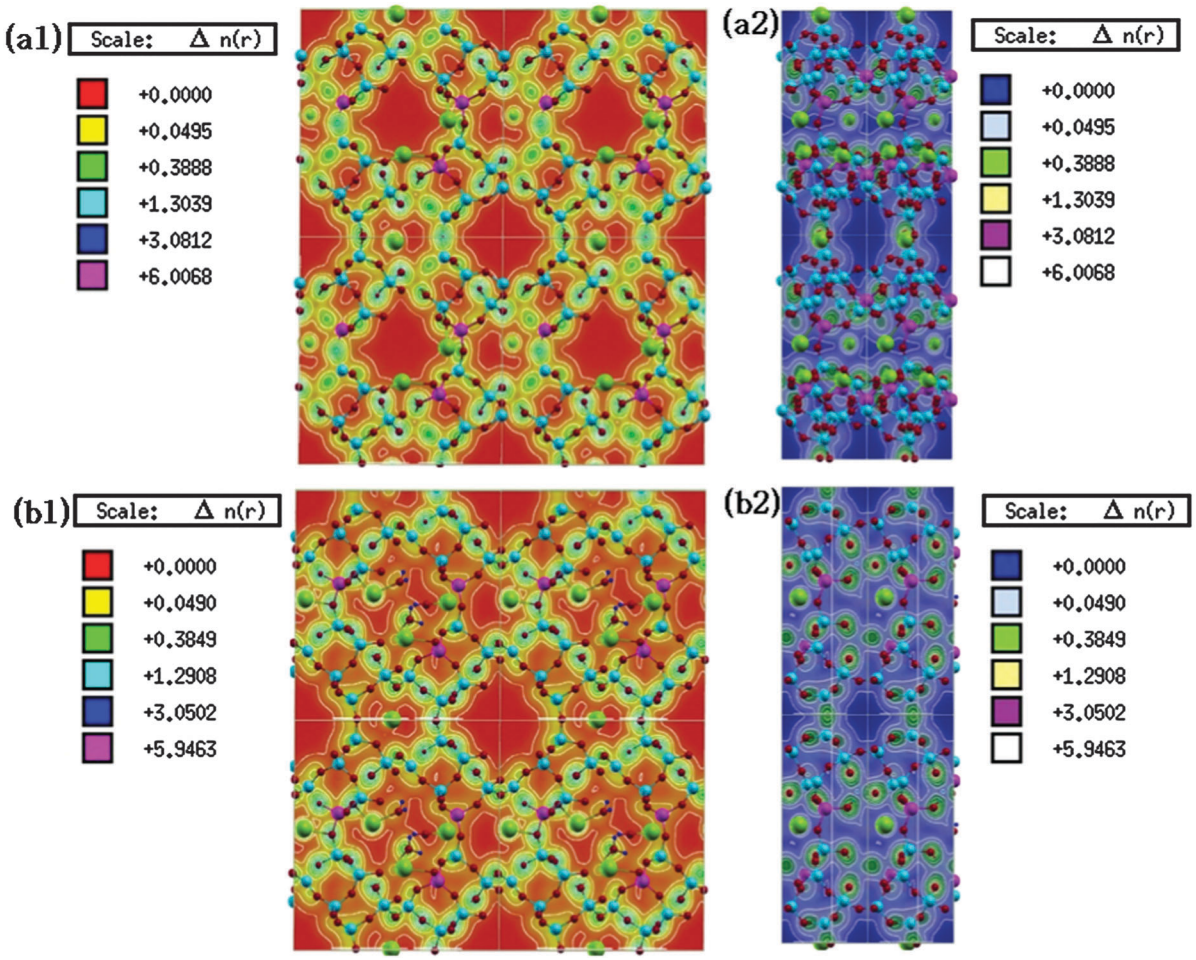

Fig. 3 The charge density distribution inside channels A, B (a1 & b1) and C (a2 & b2) for an anhydrous clinoptilolite (a) and a hydrated clinoptilolite structure (b) (Si = light blue, O = red, Al = violet, Na = green, H = dark blue).

3.3 Adsorption of arsenic

We now discuss the adsorption characteristics of arsenic acid $AsO(OH)_3$ and arsenous acid $As(OH)_3$ in the anhydrous and hydrated Al-modified CL zeolites. The structures of the optimized adsorption complexes are displayed in Fig. 4–7 and the adsorption energies at different adsorption sites as a function of the Si/Al ratio (Si/Al = 1.7, 5, 6 and 8) are summarized in Table 3, for the anhydrous and hydrated compositions. Four different adsorption sites were studied, labelled sites 1 to 4 as shown in Fig. 4–7. Site 1 is located in the 10-membered rings (channel A) containing the two preferred cation sites M1 and M4, whereas site 2 is located in the 8-membered rings (channel B) in the (001) plane and contains one cation site (M2). Site 3 is also located in the 8-membered ring, but in the (100) plane, and contains another preferred cation site (M3). Site 4 is located between the 8-membered ring in the (001) plane and the (100) plane and contains one cation site (M2). The adsorption energy of the adsorbates was calculated as follows:

$$E_{ads} = E_{zeolite+adsorbate} - (E_{zeolite} + E_{adsorbate}) \quad (1)$$

where $E_{zeolite+adsorbate}$ is the total energy of the zeolite–adsorbate system in the equilibrium state, $E_{zeolite}$ is the total energy of the zeolite framework without adsorbates, and $E_{adsorbate}$ is the total energy of the isolated adsorbate molecule. By this definition, a negative value of E_{ads} indicates an exothermic and stable adsorption, whereas a positive value indicates unstable adsorption.

Essentially, the adsorption energies for arsenous acid in the anhydrous aluminium-modified CL zeolite are favorable at all adsorption sites for different Si/Al ratios. In the case of arsenic acid, however, most of the adsorption sites lead to favorable adsorption energies, but unfavorable positive energies were obtained upon adsorption in site 3 for the Si/Al ratio of 5 and in site 4 for the Si/Al ratios of 6 and 8. A plot of the adsorption energies for the different Si/Al ratios per adsorption site is shown in Fig. 8. In the anhydrous aluminium-modified CL, the adsorption energies of $AsO(OH)_3$ and $As(OH)_3$ are found to depend sensitively on the Si/Al ratio. The strongest interaction is predicted for the Si/Al ratio of 1.7, where the preferred adsorption site was found to be site 1 in the 10-membered ring (Fig. 4a and 6a). We observe that an increase in the Si/Al ratio results in a decrease in the absolute values of the adsorption energies. It is worth noting that in the anhydrous Al-modified CL zeolite, both the $AsO(OH)_3$ and $As(OH)_3$ species generally adsorb associatively and exothermically.

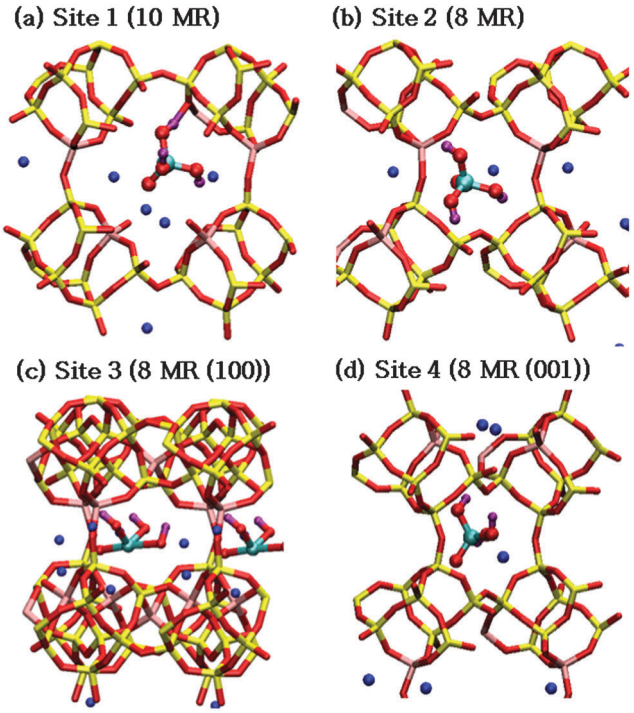

Fig. 4 The optimized adsorption complexes of $AsO(OH)_3$ at different adsorption sites in anhydrous Al-modified clinoptilolite. (Si = yellow, O = red, Al = pink, Na = blue, H = violet, As = sky blue).

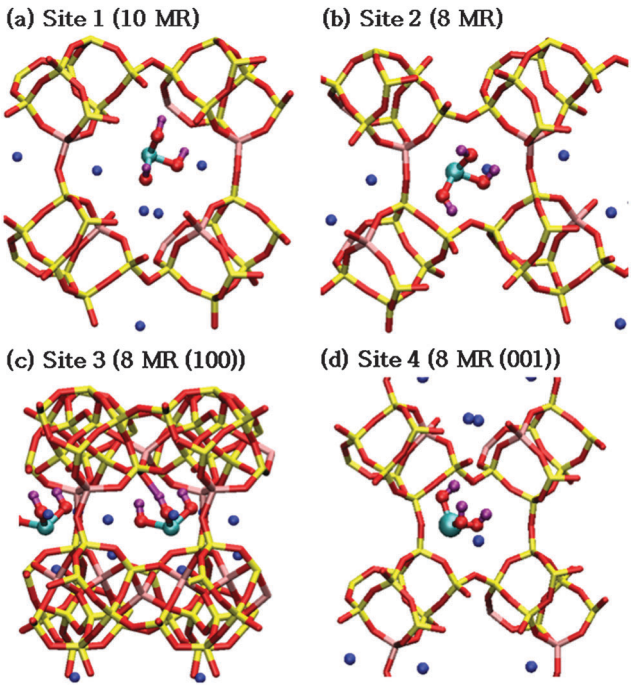

Fig. 5 The optimized adsorption complexes of $As(OH)_3$ at different adsorption sites in anhydrous Al-modified clinoptilolite. (Si = yellow, O = red, Al = pink, Na = blue, H = violet, As = sky blue).

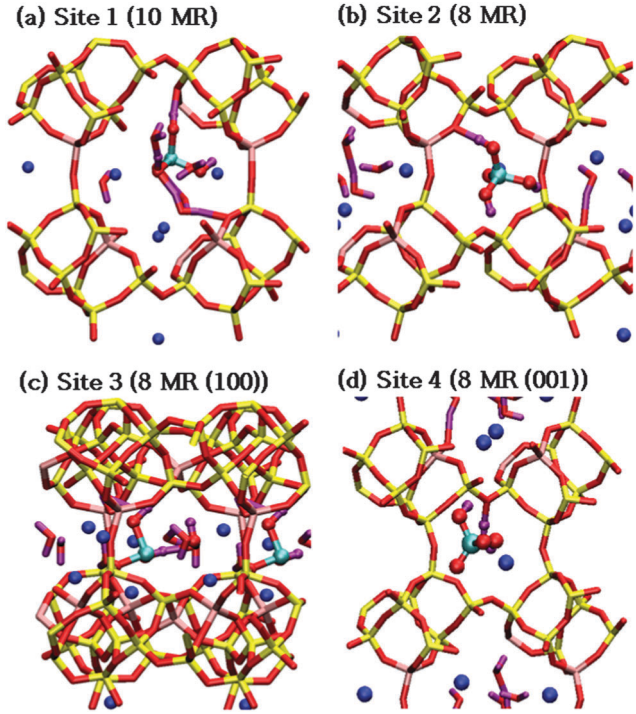

Fig. 6 The optimized adsorption complexes of $AsO(OH)_3$ at different adsorption sites in hydrated Al-modified clinoptilolite. (Si = yellow, O = red, Al = pink, Na = blue, H = violet, As = sky blue).

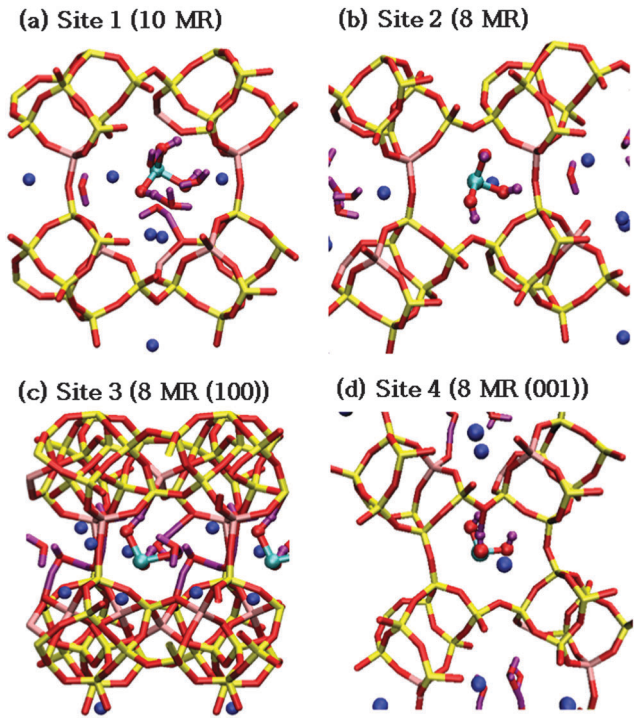

Fig. 7 The optimized adsorption complexes of $As(OH)_3$ at different adsorption sites in hydrated Al-modified clinoptilolite. (Si = yellow, O = red, Al = pink, Na = blue, H = violet, As = sky blue).

Fig. 8 depicts the trends of and relationships between the strength of adsorption at various adsorption sites as a function of different Si/Al ratios. We see that the most stable adsorption complex for both $AsO(OH)_3$ and $As(OH)_3$ in the anhydrous zeolite is obtained for the same Si/Al ratio of 1.7, but the

Table 3 Adsorption energies (kJ mol^{-1}) for $AsO(OH)_3$ and $As(OH)_3$ in anhydrous and hydrated Al-modified clinoptilolite (Si/Al ratio = 1.7, 5, 6 and 8) at different adsorption sites

	Arsenic acid ($AsO(OH)_3$)				Arsenous acid ($As(OH)_3$)			
Sites/Si/Al ratios	1.7	5	6	8	1.7	5	6	8
Anhydrous composition								
Site 1 (10 MR)	−250.6	−200.1	−97.4	−56.5	−226.3	−131.9	−163.9	−123.6
Site 2 (8 MR)	−178.0	−124.8	−123	−98.5	−108.2	−77.2	−91.5	−72.4
Site 3 (8 MR[100])	−252.4	2.2	−171.8	−143.9	−158.8	−127.8	−116.6	−117.1
Site 4 (8 MR)	−104.4	−8.2	0.1	4.9	−125.3	−70.2	−34.0	−8.0
Hydrated composition								
Site 1 (10 MR)	260.2	39.0	214.0	243.8	365.2	7.6	123.7	314.1
Site 2 (8 MR)	118.3	−156.8	−104.9	−144.1	−69.7	−139.0	−63.6	−114.7
Site 3 (8 MR[100])	193.5	150.2	173.6	205.2	64.7	−6.1	32.3	585.8
Site 4 (8 MR)	−58.5	−59.2	−32.4	−51.0	−161.1	−129.3	−68.8	−61.5

adsorption sites differ, as they are, respectively, calculated to be at site 3 in the 8 MR and at site 1 in the 10 MR. The strongest adsorption energies for $AsO(OH)_3$ and $As(OH)_3$ in the anhydrous zeolite are calculated at −252.4 kJ mol^{-1} and −226.3 kJ mol^{-1}, respectively, which suggest that the $AsO(OH)_3$ species interacts more strongly with the zeolite framework than with the $As(OH)_3$ species.

When rich in aluminium, the interaction between the Na^+ cations and the adsorbate molecules in the anhydrous CL increases, leading to larger and favourable adsorption energies. We observe an elongation of the As–O bonds from 1.745 Å to 1.774 Å and that of the O–H from 0.981 Å to 1.000 Å, which indicates that these bonds become weakened upon adsorption. This weakening of the interatomic bonds can be attributed to the small net transfer of 0.01–0.20 e$^-$ from the interacting framework atoms to the adsorbing molecules, as determined from Löwdin population analyses.[58] In contrast to the anhydrous Al-modified CL zeolite, the introduction of water molecules in the framework is found to have a destabilizing effect on the adsorption of both $AsO(OH)_3$ and $As(OH)_3$. This effect can be attributed to the competition between the water molecules and the arsenic species for cation sites. Because the water molecules fill the pores,

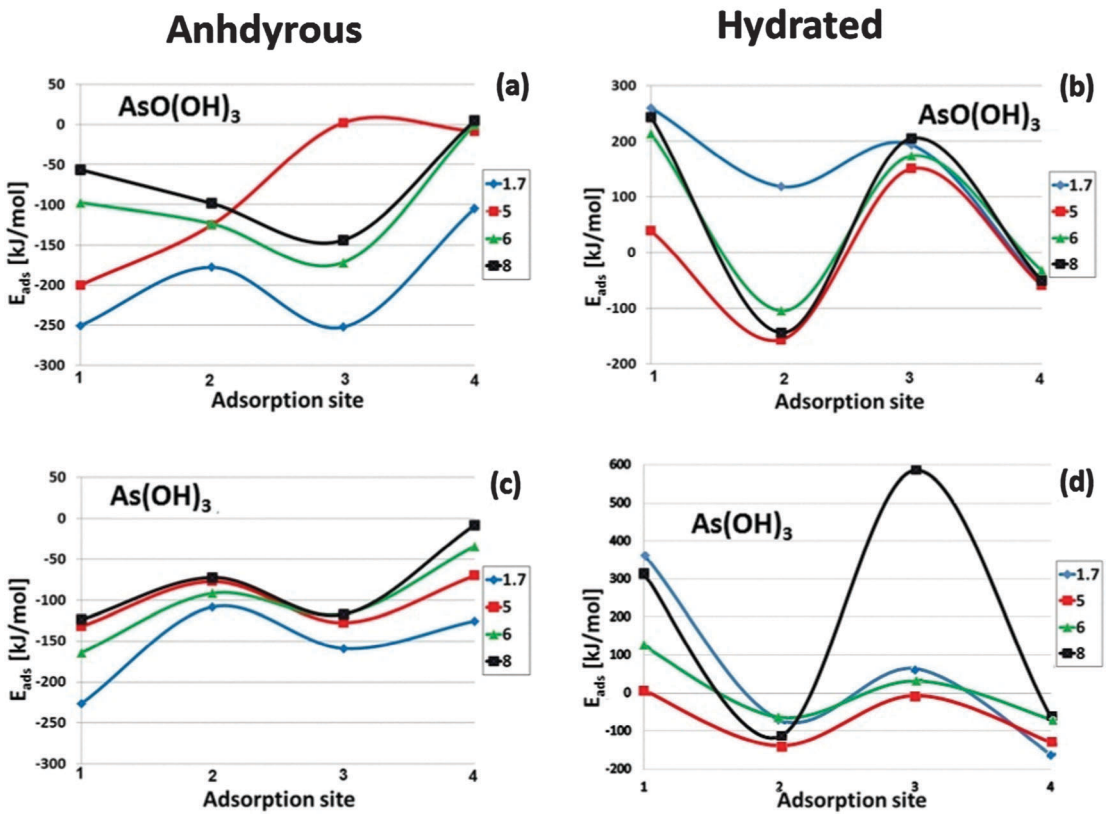

Fig. 8 Adsorption energies of $AsO(OH)_3$ and $As(OH)_3$ as a function of the Si/Al ratio (1.7, 5, 6 and 8) at different adsorption sites of anhydrous and hydrated Al-modified clinoptilolite.

they prevent the Na^+ cations from easy migration towards the arsenic species to enhance their adsorption. Prior to the adsorption of the $AsO(OH)_3$ and $As(OH)_3$ molecules, the O–H bond of the water molecules was 0.88 Å, which elongated to 1.00 Å after adsorption. At site 3, unlike in the anhydrous CL, both arsenic species adsorb dissociatively at low Si/Al ratios (1.7 and 5), *i.e.*, one OH breaks away from the As to bind to a Na^+ cation (Fig. 6), and the adsorption process was calculated to be endothermic. We observed that the adsorption is favorable at sites 2 and 4 for both $AsO(OH)_3$ and $As(OH)_3$ for all Si/Al ratios except for the ratio of 1.7. The strongest interaction, which released an adsorption energy of 156.8 kJ mol^{-1} for $AsO(OH)_3$, was predicted at site 2 for a Si/Al ratio of 5, whereas the weakest negative interaction at −32.4 kJ mol^{-1} was predicted at site 4 for a Si/Al ratio of 6. For $As(OH)_3$, the strongest (−161.1 kJ mol^{-1}) and the weakest (−61.5 kJ mol^{-1}) exothermic interactions were both calculated at site 4 for Si/Al ratios of 1.7 and 8 respectively. The adsorption site 4 with a Si/Al ratio of 1.7 contains two Na^+ cations but no water molecule to compete with the arsenic species for the active binding sites, hence the strong interaction calculated at this site (Fig. 5b and 7b). Similar to the anhydrous zeolite, we also observed an elongation of the As–O and O–H bonds in both arsenic adsorbates in the hydrated compositions. In hydrated systems, therefore, the adsorption of the As species is less exothermic, but hydrated clinoptilolite will nevertheless act as an effective adsorbent for these species according to our results. Our Löwdin population analyses of the hydrated systems with the most positive adsorption energies show that the As adsorbate species have a net positive charge (0.06–0.11 e^-), which suggests that they lose charge to the interacting framework atoms, in contrast to the anhydrous systems. The loss of charge by the arsenic species in the hydrated systems further indicates that the water molecules have a destabilizing effect on the adsorption of both arsenic species, which is consistent with the weak exothermic and endothermic adsorption energies calculated for the hydrated conditions.

4. Summary and conclusions

We have employed first-principles DFT calculations to evaluate the adsorption capacity of anhydrous and hydrated Al(III)-modified clinoptilolite zeolite for $AsO(OH)_3$ and $As(OH)_3$ species. Our calculations have shown that, when present, the framework water molecules coordinate with the cations present in the CL zeolites pores, in good agreement with the prediction of Higgins *et al.*,[53] where they reduce the charge density distribution within the pores. From the calculated adsorption energies and characteristics, we show that both species of arsenic adsorb favorably in the anhydrous Al(III)-modified CL zeolite (associative and exothermic), while in the hydrated zeolite the adsorption is less favoured and dissociative, although there are still sites where exothermic adsorption is predicted. The adsorption energies are also shown to depend sensitively on the Si/Al ratio, where a low ratio of 1.7 was shown to be preferred for the anhydrous zeolite, but the ratio of 5, which is the Si/Al ratio of naturally occurring clinoptilolite, was demonstrated to be most favourable under hydrated conditions. This work improves our understanding of the role that Al(III)-modified clinoptilolite zeolite may play in the remediation of sites contaminated by arsenic and indeed suggests that these zeolites could be effective for the immobilization of these toxic species.

As shown from the calculated structural parameters, the DFT method is capable of accurately predicting interatomic distances in comparison with experiment, but due to its static nature, it could not describe the dynamic processes in the channels of the zeolite systems, such as water dynamics, distribution and orientations. The calculated interatomic distances and binding energies from this work may also be used in the derivation of force fields which could then be employed in classical MD simulations to simulate complex systems, including single and multiple arsenic species in an explicit aqueous environment or fully hydrated systems. Future work will also include investigations of the effect of other charge compensating cations like K^+, Ca^{2+}, Ba^{2+}, Sr^{2+}, Cs^+, and Mg^{2+}, which often appear in the clinoptilolite framework, on the sorption process of the arsenic species.

Acknowledgements

The authors gratefully acknowledge the UK's Royal Society and the Leverhulme Trust for a research grant under the Royal Society-Leverhulme Africa Award Scheme. EA, RT and JBA also acknowledge the National Council for Tertiary Education, Ghana, for a TALIF research grant.

References

1 J. F. Ferguson and G. Jerome, *Water Res.*, 1972, **6**, 1259–1274.
2 D. K. Nordstrom, *Public health. Worldwide occurrences of arsenic in ground water., Science*, Washington, 296.5576 edn, 2002, vol. 296.
3 M. F. Hughes, *Toxicol. Lett.*, 2002, **133**, 1–16.
4 U. S. Environmental Protection Agency Report EPA/625, 1999.
5 U. S. Environmental Protection Angency, 2001, vol. 66.
6 F.-S. Zhang and H. Itoh, *Chemosphere*, 2005, **60**, 319–325.
7 N. Amin, S. Kaneco, T. Kitagawa, A. Begum, H. Katsumata, T. Suzuki and K. Ohta, *Ind. Eng. Chem. Res.*, 2006, **45**, 8105–8110.
8 J. Gulens, D. R. Champs and R. E. Jackson, in *Chemical Modelling of Aqueous systems*, ed. E. A. Jenne, A.C.S., 1979, pp. 81–95.
9 P. L. Smedley and D. G. Kinniburgh, *Appl. Geochem.*, 2002, **17**, 517–568.
10 P. N. Williams, A. H. Price, A. Raab, S. A. Hossain, J. Feldmann and A. A. Meharg, *Environ. Sci. Technol.*, 2005, **39**, 5531–5540.
11 M. Gallegos-Garcia, K. Ramírez-Muñiz and S. Song, *Miner. Process. Extr. Metall. Rev.*, 2012, **33**, 301–315.
12 D. Peak and D. L. Sparks, *Environ. Sci. Technol.*, 2002, **36**, 1460–1466.
13 M. Martínez, J. Giménez, J. De Pablo, M. Rovira and L. Duro, *Appl. Surf. Sci.*, 2006, **252**, 3767–3773.
14 M. Rovira, J. Gim, X. Mart, J. De Pablo, V. Mart and L. Duro, *J. Hazard. Mater.*, 2008, **150**, 279–284.

15 *Walid Elshorbagy Rezaul Kabir Chowdhury, Water treatement*, ed. K. Margeta and N. Logar, 2013, pp. 81–112.
16 B. Jovanovic, V. Vukasinovic-Pesic, D. Veljovic and L. Rajakovic, *J. Serb. Chem. Soc.*, 2011, **76**, 1437–1452.
17 D. Mohan and C. U. Pittman, *J. Hazard. Mater.*, 2007, **142**, 1–53.
18 H. Baker, A. Massadeh and H. Younes, *Environ. Monit.*, 2009, **157**, 319–330.
19 A. Chojnacki, K. Chojnacka, J. Hoffmann and H. Górecki, *Miner. Eng.*, 2004, **17**, 933–937.
20 S. Khachatryan, *Chem. Biol.*, 2014, **2**, 31–35.
21 S. M. Shaheen, A. S. Derbalah and F. S. Moghanm, *Int. J. Environ. Sci. Dev.*, 2012, **3**, 362–367.
22 J. Elizalde-González, M. P. Mattusch, W. D. Einicke and R. Wennrich, *Chem. Eng. J.*, 2001, **81**, 187–195.
23 F. A. Mumpton, *Am. Mineral.*, 1960, **45**, 351–369.
24 A. Godelitsas and T. Armbruster, *Microporous Mesoporous Mater.*, 2003, **61**, 3–24.
25 E. L. Uzunova and H. Mikosch, *Microporous Mesoporous Mater.*, 2013, **117**, 113–119.
26 K. Koyama and Y. Takéuchi, *Z. Kristallogr.*, 1977, **145**, 216–239.
27 T. Amsbruster and M. E. Gunter, *Am. Mineral.*, 1991, **76**, 1872–1883.
28 T. Amsbruster, *Am. Mineral.*, 1993, **78**, 260–264.
29 H. Faghihian and R. S. Bowman, *Water Res.*, 2005, **39**, 1099–1104.
30 Z. Li, *J. Hazard. Mater.*, 2011, **187**, 318–323.
31 S. Jevtic, S. Grujic, J. Hrenovic, N. Rajic and K. Z. Abshire, *Microporous Mesoporous Mater.*, 2012, **159**, 30–35.
32 M. Šiljeg, Š. C. Stefanović, M. Mazaj, N. N. Tušar, I. Arčon, J. Kovač, K. Margeta, V. Kaučič and N. Z. Logar, *Microporous Mesoporous Mater.*, 2009, **118**, 408–415.
33 Z. Li, *Microporous Mesoporous Mater.*, 2003, **61**, 181–188.
34 J. P. Perdew and Y. Wang, *Phys. Rev. B: Condens. Matter Mater. Phys.*, 1992, **45**, 13244–13249.
35 P. Giannozzi, S. Baroni, N. Bonini, M. Calandra, R. Car, C. Cavazzoni, D. e Ceresoli, G. L. Chiarotti, M. Cococcioni, I. Dabo, A. Dal Corso, S. de Gironcoli, S. Fabris, G. Fratesi, R. Gebauer, U. Gerstmann, C. Gougoussis, A. Kokalj, M. Lazzeri, L. Martin-Samos, N. Marzari, F. Mauri, R. Mazzarello, S. Paolini, A. Pasquarello, L. Paulatto, C. Sbraccia, S. Scandolo, G. Sclauzero, A. P. Seitsonen, A. Smogunov, P. Umari and R. M. Wentzcovitch, *J. Phys.: Condens. Matter*, 2009, **21**, 395502, http://www.quantum-espresso.org/.
36 D. Vanderbilt, *Phys. Rev. B: Condens. Matter Mater. Phys.*, 1990, **41**, 7892–7895.
37 J. Perdew, K. Burke and M. Ernzerhof, *Phys. Rev. Lett.*, 1996, **77**, 3865–3868.
38 J. D. Pack and H. J. Monkhorst, *Phys. Rev. B: Condens. Matter Mater. Phys.*, 1977, **16**, 1748.
39 M. P. A. T. Methfessel and A. T. Paxton, *Phys. Rev. B: Condens. Matter Mater. Phys.*, 1989, **40**, 3616.
40 R. Fletcher, *Practical methods of optimization*, John Wiley & Sons, 1987.
41 G. Gottardi and E. Galli, *Natural Zeolites*, Springer-Verlag, Berlin, 1985.
42 F. R. Ribeiro, *Zeolites: Science and Technology: Science and Technology.*, Springer, 80th edn, 1984.
43 E. Uzunova and H. Mikosch, *ACS Catal.*, 2013, **3**, 2759–2767.
44 A. Kokalj, *J. Mol. Graphics Modell.*, 2000, **17**, 176–179, 215–216.
45 W. Humphrey, A. Dalke and K. Schulten, *J. Mol. Graphics*, 1996, **14**, 33–38.
46 C. Baerlocher, L. B. Mccusker and D. H. Olson, *Atlas of Zeolite Framework Types*, Elsevier, Amsterdam, The Netherlands, 6th edn, 2007.
47 V. K. Cruz, A. Lam and C. M. Zicovich-Wilson, *J. Phys. Chem. A*, 2014, **118**, 5779–5789.
48 E. Martínez-Morales and C. M. Zicovich-Wilson, *Catal. Sci. Technol.*, 2011, **1**, 868–878.
49 C. M. Zicovich-Wilson, M. L. San-Roman, M. A. Camblor, F. Pascal and S. Durand-Niconoff, *J. Am. Chem. Soc.*, 2007, **129**, 11512–11523.
50 A. Arcoya, J. A. Gonzalez, G. Llabre, X. L. Seoane and N. Travieso, *Microporous Mater.*, 1996, **7**, 1–13.
51 A. Alberti, *TMPM, Tschermaks Mineral. Petrogr. Mitt.*, 1972, **146**.
52 C. Baerlocher, L. B. Mccusker and D. H. Olson, *Atlas of Zeolites Framework Types*, Amsterdam, The Netherlands, 5th edn, 2001.
53 R. L. Firor and K. Seff, *J. Phys. Chem.*, 1978, **82**, 1650.
54 H. Ohtaki and T. Radnai, *Chem. Rev.*, 1993, **93**, 1157.
55 N. W. Ockwig, R. T. Cygan, L. J. Criscentia and T. M. Nenoff, *Phys. Chem. Chem. Phys.*, 2008, **10**, 800–807.
56 P. Demontis, J. Gulín-González, H. Jobic, M. Masia, R. Sale and G. B. Suffritti, *ACS Nano*, 2008, **2**, 1603–1614.
57 F. M. Higgins, H. De Leeuw and S. C. Parker, *J. Mater. Chem.*, 2002, **12**, 124–131.
58 P.-O. Löwdin, *Adv. Quantum Chem.*, 1970, **5**, 185–199.